AIAA JOURNAL
Vol. 49, No. 9, September 2011

Experimental Validation of a Cascade Response Function for Fan Broadband Noise Predictions

Hélène Posson* and Michel Roger†
École Centrale de Lyon, 69134 Écully, France

DOI: 10.2514/1.J050728

The present paper is aimed at assessing an analytical prediction model for the broadband noise produced by the impingement of turbulence on a cascade, using a dedicated experiment. The model is a strip-theory approach based on a previously published formulation of the unsteady blade loading for a rectilinear cascade. The experimental setup is made of a single stationary cascade of vanes mounted downstream of a turbulence grid in an annular duct, at the exit of an open-jet anechoic wind tunnel. The statistical parameters of the turbulence measured with hot-wire anemometry are used as input data in the model. The in-duct predicted downstream acoustic power is compared with the measured power obtained from the far-field acoustic pressure. Measured and predicted variations of the acoustic power with the number of vanes of the cascade and with the turbulence intensity are found to be in good agreement. It is concluded that the analytical approach succeeds in highlighting three-dimensional effects and is promising for further comparisons in more complex annular configurations.

Nomenclature

B	=	number of vanes
c	=	vane chord length
Ci	=	cascade i, $i = 1$ ($B = 49$) or $i = 2$ ($B = 98$)
c_0	=	speed of sound
$E_{m,\mu}$	=	duct eigenfunction of the mode (m, μ)
$\mathbf{e}_{x_d}$	=	unit vector in the axial direction of the duct
f	=	frequency
$H_m^{(i)}(x)$	=	Hankel function of kind i of order m
$\mathbf{K}_d$	=	vector of wave numbers in the duct reference frame
K_x	=	streamwise aerodynamic wave number, ω/U_{x_d}
$(k_{x_{d0}}, k_{z_{d0}})$	=	axial and radial wave numbers of the excitation in the duct reference frame, $\mathbf{K}_{d0} = -\mathbf{K}_d$
$k_{z_{c0}}$	=	spanwise wave number in the cascade reference frame, $\mathbf{Q} \cdot \mathbf{K}_{d0}\vert_3$
k_0	=	acoustic wave number, ω/c_0
$k^{\pm}_{x,m\mu,d}$	=	axial wave number of the duct mode (m, μ)
$k^{\pm}_{x,m\mu,cd}(r)$	=	axial wave number of the duct mode (m, μ) in the cascade frame before the rotation of sweep angle
$\mathcal{L}_i$	=	measured acoustic power with a turbulence grid installed ($i =$ mes) and with no grid ($i = 0$)
$l_r(\omega)$	=	spanwise correlation length
M_{x_d}	=	axial Mach number, U_{x_d}/c_0
(m, μ)	=	azimuthal and radial orders of a duct mode
m_g	=	azimuthal order of an incident turbulent component
$\mathbf{n}_c$	=	unit vector normal to the blade
$\mathbf{Q}$	=	transformation matrix from duct to cascade reference frame, Q_{ij}
$\mathcal{R}_c$	=	reference frame attached to the rectilinear cascade at the radius r after rotation of stagger, lean, and sweep angle
$\mathcal{R}_{cd}$	=	reference frame attached to the rectilinear cascade at the radius r after rotation of stagger and lean angle
$\mathcal{R}_d$	=	stationary duct reference frame
R_H	=	hub radius
R_m	=	mean radius at midspan, $(R_T + R_H)/2$
R_T	=	tip radius
r	=	current radius
S_t	=	Strouhal number, fR_T/U_{x_d}
Ti	=	turbulence grid i, $i = 1$ ($T_u \approx 3\%$) or $i = 2$ ($T_u \approx 5.5\%$)
$T_u(r)$	=	local turbulent intensity at radius r, $u_{\text{rms}}(r)/U_x(r)$
t	=	time
$U_x(r)$	=	measured axial mean flow velocity at radius r
U_{x_d}	=	nominal value of the axial mean flow velocity at midspan
$\mathbf{u}$	=	fluctuating velocity vector in the duct stationary reference frame
u	=	streamwise velocity fluctuation
u_{rms}	=	root-mean-square value of the streamwise velocity fluctuation, $\sqrt{\overline{u^2}}$
$\mathcal{W}$	=	spectral density of the acoustic power
$w(\mathbf{x}_d, t)$	=	upwash velocity in the absolute fixed reference frame
$\check{w}(\mathbf{x}_f)$	=	upwash velocity in the fluid reference frame
$\mathbf{x}_d$	=	coordinates in the duct stationary reference frame, (x_d, r, θ_d)
β_{x_d}	=	compressibility parameter for axial mean flow
$\Gamma_{m,\mu}$	=	squared norm of the duct eigenfunction $E_{m,\mu}$
θ	=	microphone angle in the horizontal plane $\mathcal{P}$ containing the center of the exhaust section
Λ	=	turbulence integral length scale
ξ_0	=	exponential correction factor of the turbulence spectrum
ρ_0	=	fluid density
σ	=	interblade phase angle
$\Phi_{uu}(\omega)$	=	power spectral density of the streamwise velocity
$\Phi_{ww}(\mathbf{K}, r)$	=	three-dimensional wave-number turbulence spectrum for the vane normal velocity component divided by u^2_{rms}
$\hat{\varphi}$	=	sweep angle in the duct reference frame
$\hat{\chi}$	=	stagger angle in the duct reference frame
$\chi_{m,\mu}$	=	eigenvalue of the mode (m, μ)

Presented as Paper 2008-2844 at the 14th AIAA/CEAS Aeroacoustics Conference, Vancouver, Canada, 5–7 May 2008; received 30 June 2010; revision received 22 February 2011; accepted for publication 23 April 2011.

*Postdoctoral Researcher; currently Newton International Fellow, University of Cambridge, Centre for Mathematical Sciences, Department of Applied Mathematics and Theoretical Physics, Wilberforce Road, Cambridge, England CB3 0WA, United Kingdom; h.posson@damtp.cam.ac.uk. Member AIAA.

†Professor, Laboratoire de Mécanique des Fluides et Acoustique; michel.roger@ec-lyon.fr. Member AIAA.

$\hat{\psi}$ = lean angle in the duct reference frame
ω = angular frequency

I. Introduction

THE design of modern turbofan engines involves high bypass ratios for improved aircraft performance at lower nominal rotation speed. The velocity of exhaust burned gases and the jet noise are reduced, and in counterpart, fan noise becomes another important contribution to the total noise. In addition, the tonal component of fan noise is reduced and shifted to lower frequencies, due to lower fan tip speed, reduced number of blades, selected blade and vane counts, and liner optimization. As a result, the broadband noise contribution is expected to become relatively more significant. Dedicated experimental studies and prediction models are then a real need.

Many experimental studies performed in the past improved the understanding of the main noise-generating mechanisms [1] (such as rotor self-noise, rotor/stator interaction noise, the noise produced by the interaction of casing boundary layers with the blades, and the noise due to the tip leakage flow) and helped to determine their relative importance. Some works have highlighted the effects of the geometrical parameters such as the vane sweep or blade and vane counts for rotor/stator interaction noise. The most detailed investigation is the "Fan Noise Source Diagnostic Test" reported by NASA [2–5]. It deals with a stator with 54 radial vanes, a low-count stator with 26 radial vanes, and a low-noise stator with 26 swept vanes. Experiments have also been performed to validate broadband fan noise models, mainly dedicated to rotor/stator interaction noise. These experiments, dealing with small-scale or full-scale fan stages offer the advantage of being representative of a real turbomachinery fan. They are made of a full rotor/stator system, with an inlet nacelle and a standard or straight exhaust duct. The configurations remain relatively complex, since they involve several blade rows and a mean swirling flow between the rotor and the stator. Even if necessary for the validation of a complete broadband noise model, they are very expensive, require a motorization, and imply many different noise-generating mechanisms, which are hard to separate. Moreover, when studying the rotor/stator interaction noise, the rotor induces a shielding effect for the acoustic field produced on the stator and propagating upstream. Acoustic coupling between multiple blade rows and effect of swirl also occur [6]. Fundamental studies on a simple blade row are still missing.

From the point of view of sound predictions, the increased relative importance of broadband fan noise in new engines makes dedicated prediction schemes, including cascade response functions, essential for a quieter design. Numerical simulations of the turbulent compressible three-dimensional flow around the blades could accurately reproduce all sound generation and propagation phenomena, but at the price of a large computational effort, which is far from being compatible with industrial constraints. Fast-running analytical models appear to be more appropriate for the design process. In this context, an analytical model has been previously developed by the authors [7,8]. The present version of the model deals with the noise generated by the interaction of incident turbulence with an isolated annular blade row, not accounting for adjacent blade rows. It is therefore relevant to assess it against a simple experiment involving only one stationary cascade and an upstream turbulence-generation device. A setup in which only one dominant mechanism is produced is better suited for an unambiguous validation procedure, provided that all needed aerodynamic and geometric parameters can be easily measured at a reasonable cost. At the same time, it is important that the benchmark remains representative of a true axial fan technology and that the key parameters involved in the prediction model can be easily varied. Finally, the setup is designed to be used again later for further investigations. All these aspects have motivated the choice made in the present work.

The experimental setup is first described in Sec. II, and the main aerodynamic and far-field acoustic results are presented in Secs. III and IV. Finally, the downstream in-duct power predicted by the model is presented in Sec. V and is compared with the free-field power evaluated from the far-field measurements in Sec. VI.

II. Experimental Setup

The experiment is carried out in the anechoic subsonic open-jet facility of the Ecole Centrale de Lyon (dimensions $10 \times 8 \times 8$ m^3 with a 20 dBA background noise and a cutoff frequency of 100 Hz). An annular cascade made of $B = 49$ or 98 vanes is inserted downstream of a square-circular convergent nozzle at the exit section of the wind tunnel (Figs. 1 and 2). A centerbody is added for structural purposes and fixed to the wind tunnel by means of metal cables (see Fig. 1). The outer duct has a radius of $R_T = 230$ mm and ends with a thin edge (3 mm thickness) 128 mm downstream of the cascade trailing edge. The centerbody is a cylinder of radius $R_H = 150$ mm, designed with rounded ends. The inlet nose and the outlet base extend 325 mm upstream and 600 mm downstream of the cascade, respectively. This choice results from some compromise between a reasonable setup size and geometrical simplicity. On one hand, the duct is representative of the bypass exhaust duct of an engine. On the other hand, to some extent, it reproduces the model of a thin, rigid semi-infinite annular duct with an infinite centerbody addressed in Rienstra's analysis [9], at least with respect to noise-generating mechanisms that take place around the blades and radiate from the exit cross section at reasonably large frequencies. Indeed, though the present experiment associated with a minimum instrumentation is to be considered a preliminary feasibility study, future investigation of the sound scattering at the duct end is expected, possibly involving modal analysis and analytical modeling. The rounded end has been shaped arbitrarily to reduce the sudden flow separation that would occur at a straight-cylinder truncation. Vortex shedding occurs anyway and will have to be considered as a source of spurious noise. A picture of the experimental setup is shown in Fig. 1, and the main dimensions are reported in the scheme of Fig. 2. The cascade with 49 vanes is obtained by removing every second vane

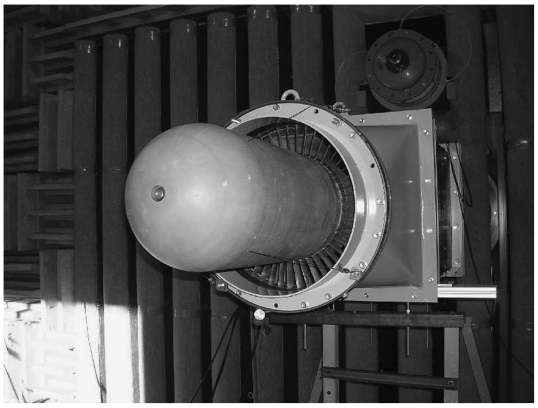

Fig. 1 Downstream view of the experimental setup.

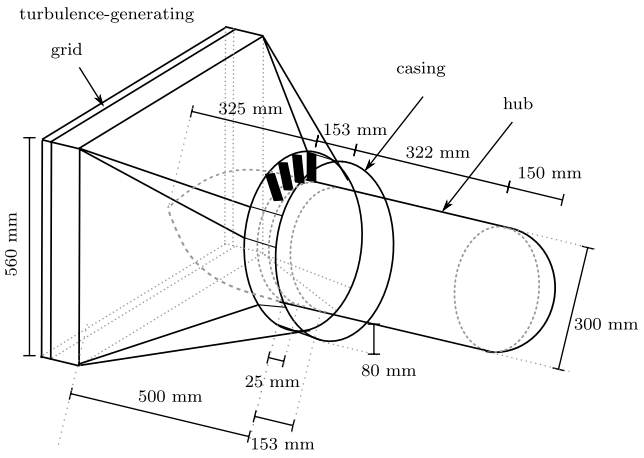

Fig. 2 Technical drawing of the experimental setup with main dimensions.

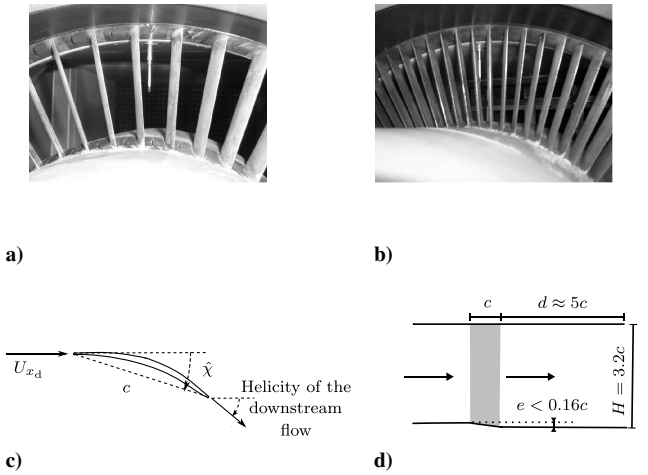

Fig. 3 a–b) photographs of the tested annular cascades showing the single-hot-wire probe for cascade C1 (solidity 1.025) and cascade C2 (solidity 2.05), respectively, c) sketch of a vane cross section showing the quasi-symmetrical shape of the vane and its direction with respect to the mean flow, and d) meridian sketch of the duct shape around the cascade.

from the initial configuration with 98 vanes. The 49 and 98 vane cascades will be referred to as cascade C1 and cascade C2, respectively, later in the paper. This leads to identical chord length $c = 25$ mm and different values of the solidity: respectively, 1.025 and 2.05 at the mean radius R_m. The angle of attack of the flow is 0° with respect to the mean camber line at leading edge, and the chord-line angle with respect to the axial direction is $\hat{\chi} = 16.7°$ (Fig. 3c). Sweep and lean are small enough to be neglected in the analysis ($\hat{\varphi}$ and $\hat{\psi}$ are assumed to be zero). Close-ups of the cascades are shown in Figs. 3a and 3b. The cascades act as inlet guide vanes inducing a swirling flow downstream. It must be noted that the original cascade is, in fact, a row of small-scale outlet guide vanes mounted back to front. Yet the vane design is almost symmetric, as shown in Fig. 3c allowing their use as inlet guide vanes, at least for the present purpose. Another issue is that the meridian cross section of the duct exhibits a small expansion, as sketched in Fig. 3d, instead of the contraction that would be obtained with the normal mounting of the cascade. The diffuser effect of the expansion might induce casing boundary-layer growth or separation in a clean-inflow configuration. However the present setup is supplied by a fully turbulent inflow for which the expansion is not expected to have any important effect.

The mean axial velocity U_{x_d} just upstream of the cascade is varied between 50 and 100 m/s. Two different turbulence-generating grids, T1 and T2, can be inserted in the wind-tunnel duct upstream of the transition toward the annular part, ensuring turbulent intensities of about 3 and 5.5%, respectively, at 30 mm upstream of the cascade. Without the grid, the residual turbulence intensity is less than 1% , which corresponds to clean-flow conditions. With no contraction downstream of a grid, homogeneous turbulence would be obtained 30 grid-mesh widths downstream, which is obviously unmanageable in the current study. The present contraction ratio 1.89 is much higher than the optimum ratio of 1.27 proposed by Comte-Bellot and Corrsin [10]. Yet, the rectangular-circular convergent nozzle with a centerbody (Fig. 2) would probably require other criteria. Therefore, the homogeneity of the turbulence just upstream of the cascade must be checked carefully. Indeed, the turbulent properties of the incident flow are required as input data in the model. If the incident turbulence on the cascade is assumed locally homogeneous and isotropic, a Liepmann or a von Kármán model spectrum tuned to single-hot-wire measurements is enough. This assumption will be discussed in Sec. III. It has been retained here for simplicity. Hot-wire-anemometry measurements are carried out using a Dantec anemometer with a Dantec 55P11 single wire, shown in Figs. 3a and 3b, at 14 radial locations in the duct cross section, every 5 mm from 5 mm below the tip radius to 6 mm above the hub, 30 mm upstream of the cascade. This provides the turbulence intensity T_u and the power spectral density (PSD) of the axial velocity Φ_{uu}. It is then possible to check the validity of the assumption of homogeneous turbulence and to evaluate the integral length scale Λ as the value giving the best fitting of the model on Φ_{uu}, at each radius. Finally, the three-dimensional spectrum Φ_{ww} of the upwash velocity w divided by u_{rms}^2 and the spanwise correlation length $l_r(\omega)$ are deduced from the turbulence model. The expressions for the homogeneous and isotropic turbulence models of von Kármán and Liepmann can be resorted to. They are found in any handbook on turbulence (see, for instance, Hinze [11]) Here, the Liepmann model has been selected.

The model to be assessed predicts the total acoustic power radiated by the impingement of incident turbulence on a blade row in an annular rigid duct, based on the propagating modes in the duct. In the experiment, acoustic far-field measurements are performed with a $\frac{1}{4}$ in. Brüel & Kjaer 4135 free-field microphone, mounted on a rotating arm. The center of the measuring arc is on axis, at the center of the exhaust cross section. The corresponding radius is 2 m, and the angle θ of the microphone is defined from the downstream setup axis. The PSD of the acoustic power is then evaluated by integrating the squared far-field pressure divided by $\rho_0 c_0$ over the arc of measurements and assuming axisymmetry. The symmetry between $\theta > 0$ and $\theta < 0$ was experimentally verified in the horizontal plane. Furthermore, the contributions from the arcs $|\theta| < 30°$ (inside the jet) and $125 < |\theta| \leqslant 180°$ (i.e., upstream) cannot be measured but are expected negligible. The level at $\theta = 120°$ was found 10 dB below the level at $\theta = 60°$, suggesting that the effectively measured power is very close to the total radiated power. It must also be noted that the sound reflection at the duct end is neglected in the present analysis. This effect could be reproduced by coupling the cascade model to diffraction calculations using Rienstra's Wiener–Hopf formulation. The reflection is only significant for cuton modes that are excited close to cutoff. As emphasized by Lordi et al. [12] for a cylindrical duct, the reflection coefficient of a mode is smaller than 0.1 well above its cutoff frequency. Therefore, in the present study, the radiated power deduced from the far-field measurements possibly underestimates the downstream acoustic power delivered by the sources inside the duct, due to the ignored reflections and the integration procedure. Yet, the underestimation is expected to be small. The absolute comparison will then be considered except around cutoff frequencies in Sec. VI.

The following terminology is introduced: Ti-Cj and C$_j$ to label the configurations with cascade j and the turbulence grid i or no turbulence grid, respectively.

III. Aerodynamic Results

The radial profiles of the mean flow velocity U_x and the turbulent intensity T_u, Fig. 4 show that a relatively thick boundary layer of around 15 mm forms on the outer wall, mainly because it originates far upstream. The boundary layer is much thinner at the hub. The turbulent intensity in the presence of a grid is found to typically decrease by 2 points from the hub to 15 mm farther away in the cross section (Fig. 4b). This is attributed to the contraction introduced by the centerbody, which accelerates the flow. Without turbulence grid, as indicated by the dotted lines in Fig. 4b, the turbulence rate is less than 1% and even around 0.2% at midheight. The acoustic measurements in that case will then be attributed to cascade self-noise (from Arbey [13] a turbulence intensity below 2% enables the study of the self-noise) and more probably to installation effects in clean flow.

The measured PSD of the axial velocity Φ_{uu} are rather well fitted by a Liepmann spectrum, as shown in Fig. 5 for the turbulence grid T2, which provides a clear value for the parameter Λ. The high-frequency decay predicted by the von Kármán spectrum would be too slow. In addition, Pope [14] proposed to introduce an exponential correction to reproduce the faster decay of the experimental spectrum at the end of the inertial range. The correction on Φ_{uu} is defined by $\Phi_{uu}^{\text{cor}}(\omega) = \Phi_{uu}(\omega) \exp(-\xi_0 K^*)$, with $K^* = K_x \Lambda$ in the Liepmann model. It improves the fit of the Liepmann spectrum. Indeed, a mean value of the exponential decay factor $\xi_0 = 0.014$ (varying from 0 to 0.020, as reported in Table 1) gives very good results.

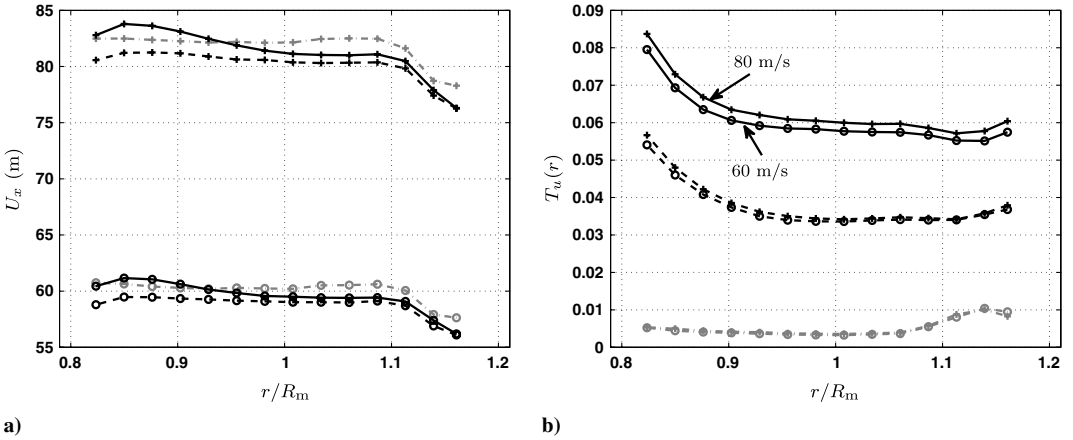

Fig. 4 Radial profiles of a) mean velocity U_x and b) turbulent intensity $T_u(r) = u_{rms}(r)/U_x(r)$. Nominal flow speeds $U_{x_d} = 60$ m/s (\circ) and 80 m/s (+). Clean-flow conditions (dot-dashed gray lines), turbulence grid T1 (dashed black lines), and turbulence grid T2 (solid black lines).

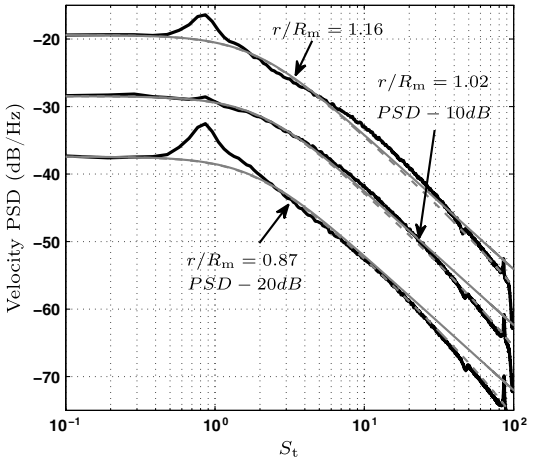

Fig. 5 PSD of the axial velocity fluctuation (in dB/Hz, velocity reference 1 m/s) as a function of the Strouhal number S_t, in configuration T2-C1 at $U_{x_d} = 60$ m/s, from measurements (thick solid black line), from the Liepmann model without correction (solid gray line), and with the exponential correction $\xi_0 \neq 0$ (dashed gray line), where the integral length Λ and the correction factor ξ_0 are given in Table 1. The groups of plots corresponding to different radii are shifted vertically by 10 dB for clarity.

The experimental setup does not involve a perfectly homogeneous turbulence, in the sense that, near the walls, for $R_H < r \leqslant R_H + 20$ mm and $R_T - 20 < r \leqslant R_T$ mm, the hot-wire spectrum exhibits a hump around $S_t = 0.73$ and 0.82 with grids T1 and T2, respectively, where S_t is the Strouhal number based on the outer radius R_T and the mean velocity U_{x_d} ($S_t = fR_T/U_{x_d}$). The amplitude of this hump increases as the probe approaches the wall, particularly near the hub as seen in Fig. 5, and can reach 4.5 and 8 dB in the worst cases for the grids T2 and T1, respectively. The hump is attributed to a spurious disturbance from the edges of the turbulence grid itself. It is important for $S_t \in [0.6, 1.15]$ and has a small contribution for $S_t \in [1.15, 1.7]$, near the hub. However, it does not contaminate the frequency range that will be retained for the acoustic analysis in Secs. IV and VI. Finally, the Liepmann spectrum is used in the model, and the root-mean-square value u_{rms} corresponding to the spectrum cleaned from the hump is retained to get a more relevant value of Λ. Table 1 reports the parameters of the turbulence for the two grids T1 and T2.

The similarity of T_u and of the spectrum Φ_{uu} has been verified for the two tested flow speeds. Furthermore, the spectra measured at two diametrically opposite angles in the same cross section coincide, proving the axisymmetry of the flow. Finally, the hot-wire-anemometry measurements have been performed with the two cascade configurations. A good repeatability of the measurements made in presence of cascade C1 and cascade C2 was expected, but the turbulent intensity T_u is increased by 9%, and the integral length scale Λ is reduced by 30% when changing from configuration C1 to configuration C2. The hot-wire probe sensitivity to some cascade potential effect is not probable, since it has been placed 1.2 chord upstream of the cascade. Another explanation is the change of pressure rise induced by the change of solidity of the cascade, possibly responsible for a different development of the grid turbulence.

IV. Acoustic Results

The PSD of the radiated power as deduced from the far-field measurements, noted $\mathcal{W}$, has been determined for incident flow speeds U_{x_d} ranging from 50 to 100 m/s by steps of 10 m/s for all configurations. $\mathcal{W}$ is found to scale like $U_{x_d}^n$ with $n = 5$ to 6 when plotted as a function of the Strouhal number S_t in [1, 30], as shown in Fig. 6 for two configurations. More precisely, the exponent n of the scaling law $U_{x_d}^n$ is around $n = 5.5$ to 6 for low frequencies ($S_t \in [0.3, 0.9]$) and close to $n = 4.8$ for high frequencies ($S_t \geqslant 30$). It is worth noting that the fifth-power scaling on the PSD means that the overall intensity scales like $n = 6$, which is typical of broadband compact dipolelike sources attached to a solid body in a flow.

A. Inferred-Noise Mechanisms

A relevant comparison of the experimental results with model predictions requires a clear identification of the different acoustic mechanisms involved in the measurements, either related to the

Table 1 Characteristics of the turbulence produced by the grids T1 and T2 corresponding to the indices

r/R_m	0.82	0.85	0.87	0.93	0.95	0.98	1.00	1.03	1.06	1.08	1.11	1.14	1.16	1.19
$T_{u,1}$, %	4.63	4.07	3.87	3.78	3.68	3.61	3.63	3.60	3.53	3.49	3.36	3.18	3.14	3.22
Λ_1, mm	23	21	20.5	19	17.5	17	17	16	16	16	15.5	15	16	17
$100\xi_{0,1}$	1.4	1.4	1.4	1.4	1.4	1.4	1.4	1.4	1.4	1.3	1.3	1.0	0.0	0.0
$T_{u,2}$, %	6.87	6.33	6.06	6.03	6.20	6.09	6.05	6.00	5.96	5.97	5.86	5.71	5.31	5.46
Λ_2, mm	23	23	22	20	20	19	19	19	19	19	19	17	19	19
$100\xi_{0,2}$	2.0	2.0	2.0	2.0	1.8	1.8	1.8	1.8	1.7	1.6	1.5	1.3	1.3	1.0

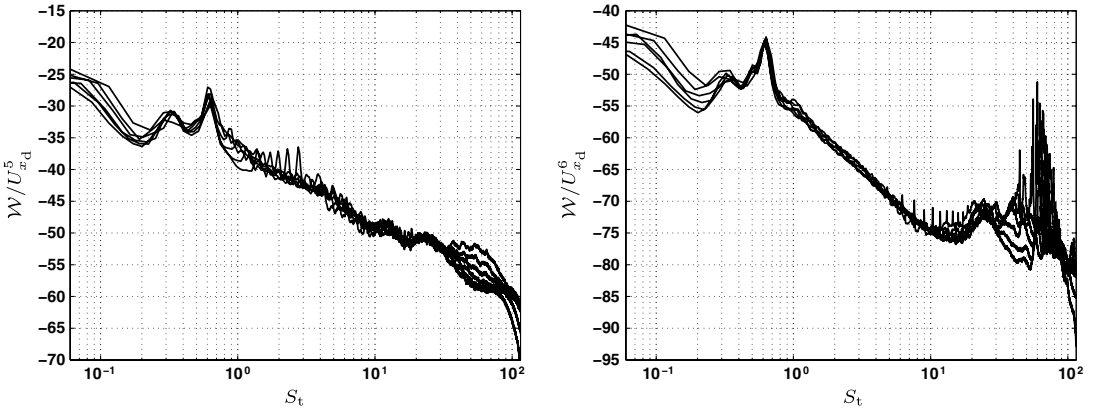

Fig. 6 PSD of the acoustic power $\mathcal{W}$ as a function of the Strouhal number S_t: a) normalized by $U_{x_d}^5$ for the configuration T2-C1 and b) normalized by $U_{x_d}^6$ for configuration C1.

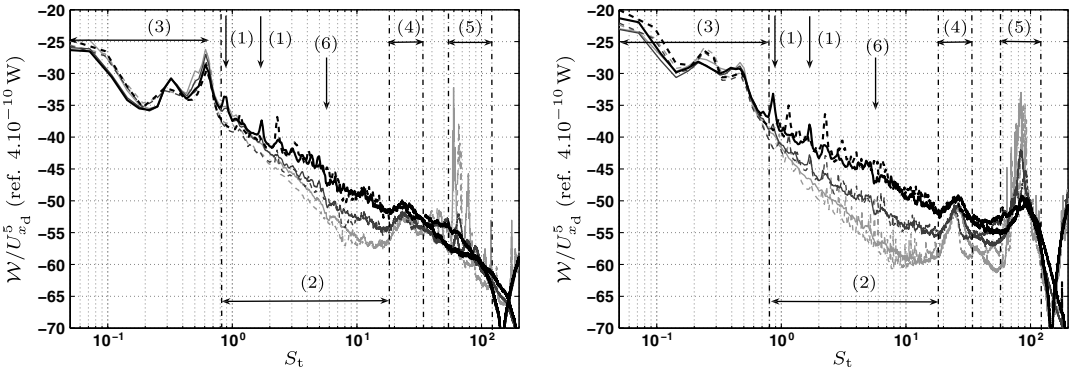

a) b)

Fig. 7 PSD of the acoustic power normalized by $U_{x_d}^5$ as a function of the Strouhal number S_t for $U_{x_d} = 60$ m/s (dashed line) and $U_{x_d} = 80$ m/s (line), with no turbulence-generating grid (thin gray line), with grid T1 (thin dark gray line) and grid T2 (thick black line): a) cascade C1 and b) cascade C2.

installation or to the investigated turbulence-interaction noise from the cascade. In view of the small residual turbulence intensity of the wind tunnel, the noise measured without grid is attributed to setup spurious sources and to blade self-noise. In fact, the spurious sources dominate self-noise over the most part of the spectrum. They can be due to the free shear layers of the jet (the swirling exhaust flow is unstable in all directions) to the outer-duct trailing-edge noise, to vortex shedding at the rounded end of the centerbody, to the flow on the cables or to separation downstream of the cascade because of the small expansion. The no-grid configurations will be taken as a reference without paying attention to a detailed breakdown on the aforementioned mechanisms, and the turbulence-interaction noise will be assessed from its emergence with respect to that reference. The emergence is around 3, 8, and 5 dB in the range of Strouhal numbers [1.75,29] for the configurations T1-C1, T2-C1, and T1-C2, respectively, and around 10 dB in [0.9,29] for T2-C2, as shown in Fig. 7 for $U_{x_d} = 80$ m/s. In view of the results, the present investigation is reliable above $S_t = 1.75$ (i.e., $f \approx 0.6$ kHz at

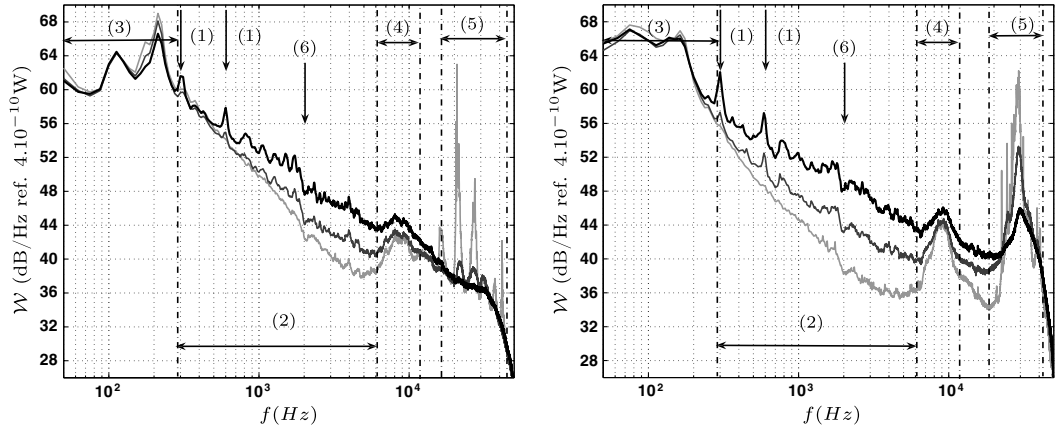

a) b)

Fig. 8 PSD of the acoustic power [dB/Hz (reference 4×10^{-10} W)] for $U_{x_d} = 80$ m/s, with no turbulence-generating grid (thin gray line), with grid T1 (thin black line) and grid T2 (thick black line): a) cascade C1 and b) cascade C2.

$U_{xd} = 80$ m/s). However, data between 0.9 ($f \approx 0.3$ kHz) and 1.75 ($f \approx 0.6$ kHz) could also make sense, despite the very weak emergence.

Different acoustic signatures are identified on the acoustic power spectra. A large low-frequency bump first dominates for $S_t < 0.8$ within the range (label 3) in Figs. 7 and 8. This contribution is found to be independent of the amount of upstream turbulence. It is attributed to large-scale oscillations of the jet interacting with the duct end and possibly vortex shedding from the centerbody termination. Indeed, a significant swirl of the exit flow has been noted, explained by the stagger angle and the camber of the vanes. The set of results with cascade C1 exhibits a peak around $S_t = 0.6$ and a less pronounced one at $S_t = 0.3$ in Fig. 7a. This signature is shifted to lower frequencies with cascade C2 (Fig. 7b), which only differs in a lower specific load because of its larger solidity. Therefore, the different low-frequency humps might be related to different mean swirling exhaust flows.

A hump is observed at high frequencies for $S_t \in [20, 30]$ in the area noted as label 4 in Figs. 7 and 8. The hump is attributed to the interaction of the exhaust swirling flow with the cables near their fixing on the hub.

Above $S_t > 55$, reported as label 5 in Figs. 7 and 8, sharp tones are produced in configurations with no turbulence-generating grid: (C1) and (C2). This mechanism radiates in the whole angular slot $\theta \in [40, 100]^\circ$ with a hardly noticeable directivity. For cascade C1 (Figs. 7a and 8a), the amplitude of the tones exceeds the broadband noise by 20 to 30 dB, with no evidence of a background hump. For cascade C2, the tones emerge by 10 dB from a hump ($f \in [20, 40]$ kHz), the height of which reaches 25 dB at 30 kHz (Figs. 7b and 8b). When the turbulence grid T1 ($T_u \approx 3\%$) is installed, the tones disappear, but for cascade C2 the amplitude of the hump is about 12 dB and drops to 5 dB with the second grid ($T_u \approx 5.5\%$). This behavior suggests a mechanism similar to Tollmien–Schlichting instabilities in the cascade. In principle the Tollmien–Schlichting mechanism corresponds to a coupling between instabilities that develop in the laminar boundary layer of an isolated vane and the feedback of the acoustic waves that are radiated upstream because of the diffraction of the instabilities at the trailing-edge. In a cascade configuration, acoustic feedback is also expected from sound reflections on adjacent blades. The frequencies of the tones are consistent with a feedback length smaller than the chord. Higher frequencies and higher amplitudes for cascade C2 may be due to different feedback conditions influenced by the neighboring blades and the different mean loading. The remaining hump on cascade C2 with the grids T1 and T2 is unexpected. Indeed, it is argued by Arbey [13] that an incident turbulence intensity of $T_u = 2.5\%$ suppresses the Tollmien–Schlichting waves on an isolated airfoil. Another possible explanation is a cascade resonance [15–17]. The tonal noise of the cascades has not been further investigated because it is out of the scope of the present study.

Finally, the behaviors in the frequency bands (label 3 to label 5) cannot be attributed to the mechanism of turbulence interaction with the cascade. For this, they are rejected here. The intermediate band of frequencies [0.3,6] kHz for $U_{x_d} = 80$ m/s, reported as label 2 in Fig. 8, is retained later. The relevance of the comparison in the frequency range [6,20] kHz will be discussed in the following sections. Specific features are observed at precise frequencies instead of Strouhal numbers in the frequency range (label 2), such as a sudden decrease at $f = 2$ kHz (label 6 in Figs. 7 and 8), most of which are seen for all grids and velocities.

B. Correction of the Measured Spectra

The sharp peaks noted as label 1 in Figs. 7 and 8 do not depend on flow speed U_{x_d}. They correspond to the cutoff frequencies of the propagation modes (1,0) and (2,0) in the annular duct. Inspection of Fig. 8 shows that they are not observed in the noise spectra measured in the absence of turbulence grid. Yet the low-frequency hump (label 3) is unchanged. Since it is observed in the clean-inflow conditions, it cannot be attributed to sources inside the duct and, in particular, to the blade trailing-edges. This confirms that another source dominates at low frequencies, for instance, trailing-edge noise from the annular exhaust lip of the duct end. In contrast, the aforementioned cutoff peaks (label 1) observed when upstream turbulence grids are installed can only be excited by in-duct sources and are certainly related to the investigated turbulence-interaction noise of the cascade. Finally, the low-frequency hump is not correlated to the noise from the cascade and must be discarded from the present analysis. In counterpart, this reduces the frequency range in which the experiment can be used to assess the model, since the hump contaminates the spectrum up to 600 Hz. This justifies a subtraction procedure defined as follows, assuming that what is considered the spurious noise sources is independent of the cascade noise of interest. The acoustic power measured with a turbulence grid installed is the sum of the turbulence-interaction noise of the cascade and of the spurious noise. It leads to the level $\mathcal{L}_{\text{mes}}$ in decibels. In clean-flow configuration, the measurements produce the level $\mathcal{L}_0$. Provided that the latter remains below the former, the noise from the cascade is expressed as

$$\mathcal{L}_c = \mathcal{L}_{\text{mes}} + 10\log_{10}(1 - 10^{(\mathcal{L}_0 - \mathcal{L}_{\text{mes}})/10}) \tag{1}$$

The correction holds as long as the difference $\mathcal{L}_{\text{mes}} - \mathcal{L}_0$ remains well positive, and it becomes negligible for a difference of about 10 dB. Associated with the far-field integration, the subtraction procedure a priori underestimates the radiated power. For this reason, the actual value of that power more probably lies between the uncorrected and corrected results. In the same way, this procedure will modify the spectrum in the areas noted as label 4 and label 5. In these frequency ranges, the humps, observed in all configurations, are attributed to spurious noise. The subsequent analysis of cascade effect on the turbulence-interaction noise is performed in the frequency range of $f \in [0.3, 20]$ kHz with the corrected spectrum. In the frequency range of [6, 20] kHz, the comparisons will not allow a definitive assessment of the models, due to the large contamination of

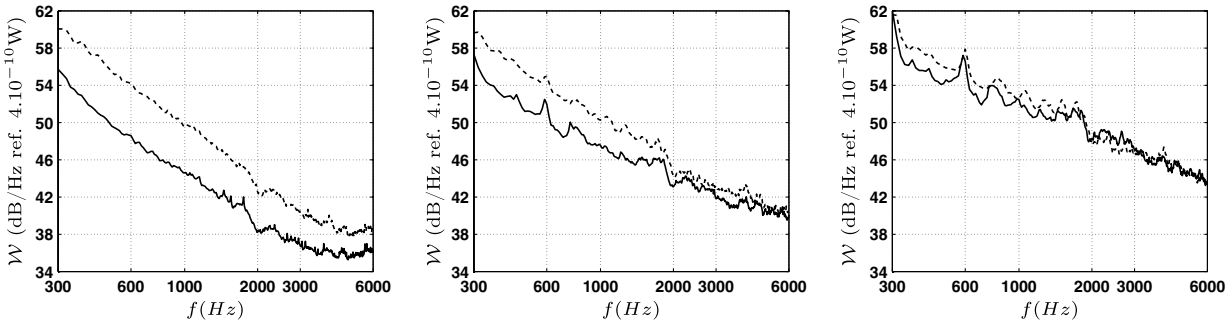

Fig. 9 PSD of the acoustic power [dB/Hz (reference 4×10^{-10} W)] at $U_{x_d} = 80$ m/s for cascade C1 (dashed line) and cascade C2 (solid line): a) with no turbulence-generating grid, b) with grid T1, and c) with grid T2.

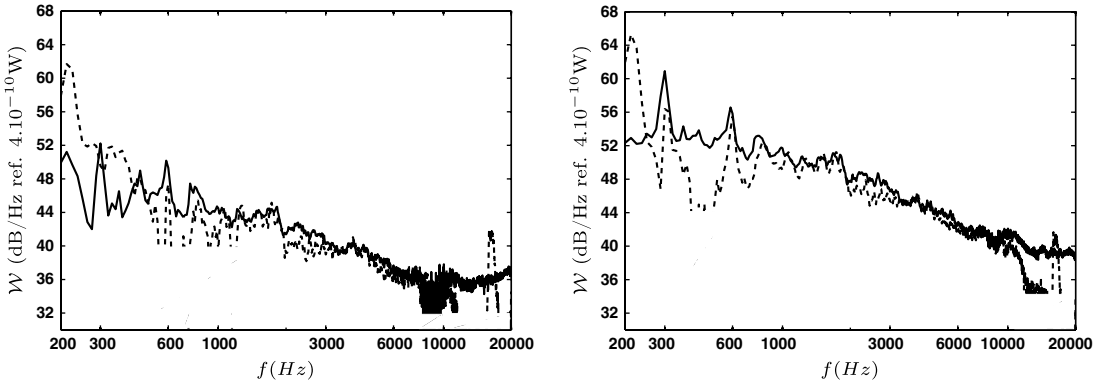

Fig. 10 PSD of the corrected acoustic power $\mathcal{L}_c$ [dB/Hz (reference 4×10^{-10} W)] from Eq. (1) at $U_{x_d} = 80$ m/s for cascade C1 (dashed line) and cascade C2 (solid line) with the grid: a) T1 and b) T2.

the spectra, but will give some clues concerning their behavior. It must also be noted that the spurious noise sources are not modified when the turbulence grids are added, which might be questionable.

C. Cascade Effect

Can be defined as cascade effect any behavior that differs from a noise increase of $10\log_{10}(B_2/B_1)$ dB when increasing the number of vanes from B_1 to B_2. The two cascades are first compared in the frequency range (label 2) in Fig. 9 with no correction of the measured spectra. With no turbulence-generating grid cascade C1 is noisier than cascade C2 by about 5 dB. This suggests that the self-noise from the cascade or from the outer-duct end is higher in the configuration (C1). Both explanations are related to a higher mean loading. The values of $\mathcal{W}$ measured with turbulence-generating grids T1 and T2 are plotted in Figs. 9b and 9c, respectively. The difference of acoustic signature with increasing turbulence intensity decreases. Furthermore the frequency range over which a clear difference can be observed is reduced. cascade C2 obviously generates more sound as the level of incident turbulence increases, whereas cascade C1 appears more contaminated by self-noise. This makes the assessment of the vane-count effect on turbulence-interaction noise less easy to investigate.

Therefore, the comparison is made in Fig. 10, based on the corrected data in which the noise not attributed to the oncoming turbulence has been subtracted according to Eq. (1). Now cascade C2 is found noisier than cascade C1. This result must be interpreted with care. Indeed, the correction is questionable at low frequencies and induces an unexpected change in slope of the spectrum in the configuration (T1–C2). Two preliminary conclusions arise. On one hand, the experimental setup makes the emergence of turbulence-interaction noise limited. Increasing the oncoming turbulence intensity in future tests would highlight the investigated mechanism. Nevertheless, essentially because that turbulence is also involved in what is considered spurious noise and especially the trailing-edge noise at the outer-duct end, the issue of extracting turbulence-interaction noise would persist. It also would be relevant to design and compare different cascades having the same aerodynamic loads in order to investigate the effect of the vane number.

On the other hand, if the procedure of correction is assumed consistent the spectra of Fig. 10 are expectedly more reliable. The noise produced by the impingement of incident turbulence is shown to be higher with cascade C2 than with cascade C1 by about 1.5 to 3 dB for $f \in [0.6, 1] \cup [2, 4]$ kHz and is nearly the same for $f \in [1, 2] \cup [4, 10]$ kHz. A difference of exactly 3 dB corresponds to the effect of doubling the blade number, which means no cascade effect. Departures from this value can be attributed to that effect. Again all results are strictly valid only if the acoustic fields produced by the different mechanisms are perfectly uncorrelated. This remains a concern here, since the upstream turbulence has an effect at the duct end.

Section VI is dedicated to checking whether the observed variations with the incident turbulence are reproduced by the model.

V. Broadband Noise Model

The analytical model for the broadband noise produced by the impingement of turbulence on a cascade is based on a previous formulation for an unwrapped cascade [18,19], following Glegg's rectilinear-cascade response [20]. The model determines closed-form expressions for the induced unsteady loads. As Peake [21] pointed out, cascade near-field information such as unsteady blade loading is less sensitive to the three-dimensional annular geometry than the acoustic pressure or power farther away inside the duct. Results closer to reality are expected by evaluating the local unsteady blade loading in an equivalent rectilinear cascade and resorting to an acoustic analogy in an annular duct to propagate the sound, rather than by directly addressing the radiated field from a rectilinear-cascade configuration. The assessment of this approach precisely enters the scope of the present study. The model is quoted below as a *quasi-3-D annular model*. It resorts to a strip-theory approach [18,22]. Each radial strip of the true blade row is unwrapped and assimilated to a rectilinear cascade having the local geometrical parameters. Then the unsteady loading on the cascade is used as a dipole source distribution in the usual sense of the acoustic analogy. The sound field is expanded on the propagating modes tailored to an annular rigid duct with uniform mean flow, via a statistical analysis.

The following developments deal with turbulence convected by an axial mean flow impinging on a stationary blade row. It is a special case of the model [7] where the rotation of the blade row Ω_R is set to zero. The turbulence is described by a frozen gust pattern convected past the cascade assuming Taylor's hypothesis. In a stationary reference frame $\mathcal{R}_d$ of coordinates $\mathbf{x}_d = (x_d, r, \theta_d)$ with x_d along the duct axis, the upwash velocity is defined by

$$\mathbf{u}(\mathbf{x}_d, t) \cdot \mathbf{n}_c = w(\mathbf{x}_d, t) = \check{w}(\mathbf{x}_d - tU_x(r)\mathbf{e}_{x_d}) \tag{2}$$

where $\check{w}(\mathbf{x}_f)$ is the upwash velocity in the fluid reference frame. The assumption of locally homogeneous and isotropic turbulence allows writing $\check{w}(\mathbf{x}_d) = u_{\text{rms}}(\grave{r})\bar{w}(\check{\mathbf{x}}_d, \grave{r})$, where $\bar{w}$ is the nondimensional upwash velocity, and the symbols above coordinates are only to note that the amplitude u_{rms} and integral length scale Λ of the turbulence vary with the reference radius r but that the turbulence itself is nearly isotropic in a vicinity of this radius. $\grave{r} = r/R_T$ accounts for slow variations of the turbulence from one strip to a neighboring one, whereas $\check{\mathbf{x}} = \mathbf{x}/\Lambda$, which varies rapidly, is used to describe the local homogeneity and isotropy of the turbulence around a radius. Then a Liepmann model is assumed to describe the spectrum of the nondimensional velocity $\bar{w}(\check{\mathbf{x}}_d, \grave{r})$. Since the turbulence is analyzed in a duct, $\check{w}(\mathbf{x}_f)$ and then $w(\mathbf{x}_d, t)$ are periodic functions of the azimuthal angle. The definition of the Fourier transform yields

$$\check{w}_{m_g}(k_{x_d}, k_{z_{d0}}, \omega) = \tfrac{1}{(2\pi)^4}\int_{-\infty}^{\infty}\iint_{\mathbb{R}^2}\int_{-\pi}^{\pi} w(\mathbf{x}_d, t)e^{i\omega t + ik_{x_d}x_d - im_g\theta_d - ik_{z_{d0}}r}\,\mathrm{d}\theta_d\,\mathrm{d}r\,\mathrm{d}x_d\,\mathrm{d}\omega \tag{3}$$

Now the expected values of turbulent quantities must be introduced. After developments in a rather similar way as in Ventres et al. [23], the upwash expected value $S_{WW} = \langle w_{m_g}(k_{x_d}, k_{z_{d0}}, \omega)\, w_{m_g'}(k'_{x_d}, k'_{z_{d0}}, \omega')\rangle *$ is written as

$$S_{WW} = \frac{u_{\mathrm{rms}}(\grave{r})2}{r}\delta(\omega - k_{x_{d0}}U_{x_d}(\grave{r}))\delta(\omega' - \omega) \times \delta(k_{x_{d0}} - k'_{x_{d0}})\delta_{mg,mg'}\,\delta(k_{z_{d0}} - k'_{z_{d0}})\Phi_{ww}(\mathbf{K}_{d0}, \grave{r}) \tag{4}$$

where Φ_{ww} is the three-dimensional spectrum of the nondimensional upwash velocity $\bar{w}$ expressed by the Liepmann model [11] and $\mathbf{K}_{d0} = (k_{x_{d0}}, -m_g/r, k_{z_{d0}})$ with $k_{x_{d0}} = -k_{x_d}$. This result also supposes that Λ is small compared with the radial variation of the excitation, i.e., that the two radii can be taken equal in the amplitude terms.

The expression for the PSD of the acoustic power is then developed. The cross spectrum of the unsteady blade loads is assumed to go to zero as the radial distance between the two points exceeds a distance L_r such that the cascade geometry and the flow properties can be considered unchanged over $l_r = 2L_r$. Finally, the PSD of the amplitude of the duct mode (m, μ) is approximated by the expression

$$\langle|\mathcal{P}^{\pm}_{m,\mu}(\omega)|^2\rangle = \left(\frac{B\rho_0 c_0}{2|\kappa_{m\mu}|\Gamma_{m\mu}}\right)^2 \times \int_{R_H}^{R_T}\frac{u_{\mathrm{rms}}(\grave{r})2}{rU_{x_d}}\zeta^{\pm *}_{m,\mu}S^{\pm}_{m,\mu}(\grave{r},\omega)\sum_{m_g\in\mathbb{Z}}\sum_{k\in\mathbb{Z}}\delta_{m,mg,kB} \times \int \Phi_{ww}(\mathbf{K}_{d,0}, \grave{r})|Idp_{c,m,\mu}(\grave{r},\omega,k,k_{z_{c0}})|^2\{C^*_{m,\mu}H^{(1)*}_m(\chi_{m,\mu}r) \times \mathrm{Int}(\grave{r}, K_1) + D^*_{m,\mu}H^{(2)*}_m(\chi_{m,\mu}r)\mathrm{Int}(\grave{r}, K_2)\}\,\mathrm{d}r\,\mathrm{d}k_{z_{d0}} \tag{5}$$

where $\mathrm{Int}(\grave{r}, K_i) = 2L_r\mathrm{sinc}([K_i - k_{z_{R0}}]L_r)$, and sinc is the analytic continuation on $\mathbb{R}$ of the function $x \mapsto \sin(x)/x$ defined on $\mathbb{R}*$. l_r should be the radial correlation length of the unsteady blade loading and is taken in practice as the radial correlation length of the incident turbulence. The expressions of K_1, K_2, $\mathbf{K}_{d,0}$, and other variables in Eq. (5) are given in Appendix A. The summation over k replaces the summation over the excitation azimuthal order m_g by taking into account the condition $m - m_g \equiv 0[B]$, which corresponds to Tyler and Sofrin's condition [24]. Finally, the PSD of the acoustic power is written as follows:

$$\mathcal{W}^{\pm}(\omega) = \mp\sum_m\sum_\mu F^{\pm}_{m,\mu}\langle|\mathcal{P}^{\pm}_{m,\mu}(\omega)|^2\rangle \quad \text{with}$$

$$F^{\pm}_{m,\mu} = \pm\frac{\omega\Gamma_{m,\mu}}{\rho_0 c_0^2}\frac{\beta^4_{x_d}\Re\{\kappa_{m,\mu}(\omega)\}}{|k_0 \pm M_{x_d}\kappa_{m,\mu}(\omega)|^2} \tag{6}$$

In addition, Hanson's rectilinear formulation [25] based on Glegg's cascade model [20] has been coded and is used for comparison in Sec. VI.

VI. Comparison of Measured and Predicted Results

The statistical parameters of the incident turbulent flow as deduced from the hot-wire measurements are used as input data of the analytical model. The predictions are then compared with the acoustic power reconstructed from the far-field measurements. The Helmholtz numbers based on the chord in the test case are smaller than 3. The low-frequency limit of the model is specified by the numerical truncation of the infinite matrix system coupling the leading edges and trailing edges, since Glegg's cascade response function [20] gives the exact solution for an infinitely thin flat-plate cascade of finite length. However, using Richardson's procedure together with 100 terms in the matrix gives well-converged results. The good accuracy well below the low-frequency limit of a two-step Schwarzschild procedure has already been outlined in the limit case of a reduced cascade effect [19].

The spectra computed from Eqs. (5) and (6) exhibit sharp peaks featured by the gray line in Figs. 11a and 11b. In particular, the model predicts high level jumps at the cutoff frequencies of duct modes, such as $(m, \mu) = (1, 0)$, (2,0), (3,0), and (10,0). The corresponding peaks must be distinguished from others because they are expected from the modal formalism in a duct [26] even though their amplitude is clearly overestimated. The first cutoff frequencies of the duct modes are reproduced in Table 2 in the case where $U_{xd} = 80.4$ m/s and $c_0 = 337.8$ m/s. Some peaks are also observed in the measured spectra at the cutoff frequencies of the modes (1,0), (2,0), (3,0) but with a much lower emergence (less than 2 dB). First, as outlined in Sec. II, near the cutoff frequency of a duct mode, the reflection coefficient at the end of the duct is high, leading to a reduction of the radiated power by comparison with the in-duct power. Second, as a duct mode turns cuton ($f = f_{c,m,\mu}$), the factor $\kappa_{m,\mu}$ in the denominator of the modal coefficient in the duct according to the acoustic analogy goes to zero. In counterpart, when a cascade mode turns cuton, a cascade model for the unsteady blade loading predicts a cancellation of this mode with the same mathematical behavior as $\kappa_{m,\mu}$. As a consequence, the result remains finite in principle and is

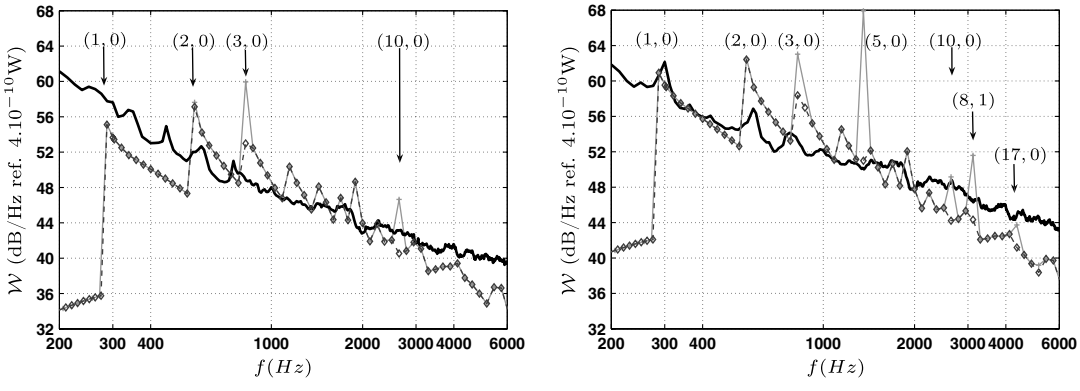

Fig. 11 PSD of the acoustic power [dB/Hz (reference 4×10^{-10} W)] at $U_{x_d} = 80$ m/s with cascade C2: from experimental data (thick black line), from the quasi-three-dimensional formulation (thin gray line with +) and from the improvement of the quasi-three-dimensional formulation (dashed black line with ◇): a) T1-C2 and b) T2-C2.

Table 2 Cutoff frequencies (in Hz) of the first duct modes for $U_{xd} = 80.4$ m/s and $c_0 = 337.8$ m/s

(m, μ)	(1,0)	(2,0)	(3,0)	(4,0)	(5,0)	(6,0)	(7,0)	(0,1)
$f_{c,m,\mu}$	276	551	825	1096	1364	1628	1889	2090
(m, μ)	(1,1)	(8,0)	(2,1)	(3,1)	(4,1)	(9,0)	(5,1)	(10,0)
$f_{c,m,\mu}$	(6,1)	(11,0)	——	(8,1)	——	(17,0)	——	——
$f_{c,m,\mu}$	2718	2894	——	3116	——	4346	——	——

expected to vary regularly. It is so when using an acoustic analogy in rectilinear configuration (Green's function for rectilinear configuration) with the present model of blade loading. It would be so as well with a fully three-dimensional annular-cascade response function, accounting for the real geometry and applying the acoustic analogy in an annular duct, in the same way as with the three-dimensional seminumerical models of Namba [27] or Schulten [28], or with a code solving the three-dimensional linearized Euler equations [29]. Hanson's approximation does not exhibit any singularity, since its direct-radiation formulation is equivalent to an acoustic analogy in a rectilinear configuration and since the present unsteady blade loading is suited to rectilinear cascades. Here, the singularity arises because a mixed formulation is used. The rectilinear-cascade cutoff frequencies do not in general fit with the duct-mode cuton frequencies, especially in a broadband calculation procedure scanning all real spanwise wave numbers. Some spurious peaks can be reduced by forcing the rectilinear cascade to work at the cascade cuton frequency of the mode m when the investigated frequency is close to the duct cuton frequency of a mode (m, μ). This is achieved by imposing the spanwise wave number $k_{z_{c0}}$ of a gust in order to get the equality of cuton frequencies. Namely, for an incident gust of azimuthal order m_g, the cutoff angular frequency of the duct mode $\omega_{c,m,\mu}$ and the cutoff angular frequency of the rectilinear-cascade diffracted mode of azimuthal order q, with $m = m_g + qB$, $\omega_{\mathrm{ex},c,q}$ must coincide. The expression of $k_{z_{c0}}$ to get $\omega_{\mathrm{ex},c,q}(k_{z_{c0}}) = \omega_{c,m,\mu}$ is detailed in Appendix B in the case of zero sweep and lean angles $\hat{\varphi} = \hat{\psi} = 0°$. It artificially selects this contribution but enables to notably remove some spurious peaks from the spectra, as shown in Fig. 11. The remaining peaks are numerical artefacts inherent to the approach for which an improvement is currently under investigation. Next comparisons are all performed with the corrected model.

The results from the quasi-3-D annular formulation and from the coding of Hanson's formulation [25,30] are plotted against the measured PSD in Figs. 12 and 13 for cascade C2 and C1, respectively, and the two turbulence grids. For cascade C2, in Fig. 12, Hanson's formulation is in rather good agreement with the experimental data, both in terms of relative variations between the two grids and in terms of absolute levels for $f \in [0.6, 5]$ kHz, with discrepancies smaller than 2 dB. This suggests that this fast-running approximation can be used for an annular cascade and probably for blades of more complex geometry by using a strip theory, as shown by the study [25] on the advanced ducted propulsor benchmark of NASA/Pratt & Whitney.

The two discontinuities produced by the models between 271 and 284 Hz and between 528 and 558 Hz correspond to the cutoff frequencies of the duct modes $(m, \mu) = (1, 0)$ ($f_{c,1,0} = 276$ Hz), and $(m, \mu) = (2, 0)$ ($f_{c,2,0} = 551$ Hz) at $U_{xd} = 80$ m/s. Though exaggerated with respect to the measurements, they are associated with the aforementioned physical aspects. The discontinuities are stronger at low frequencies. Indeed, at higher frequencies, the high

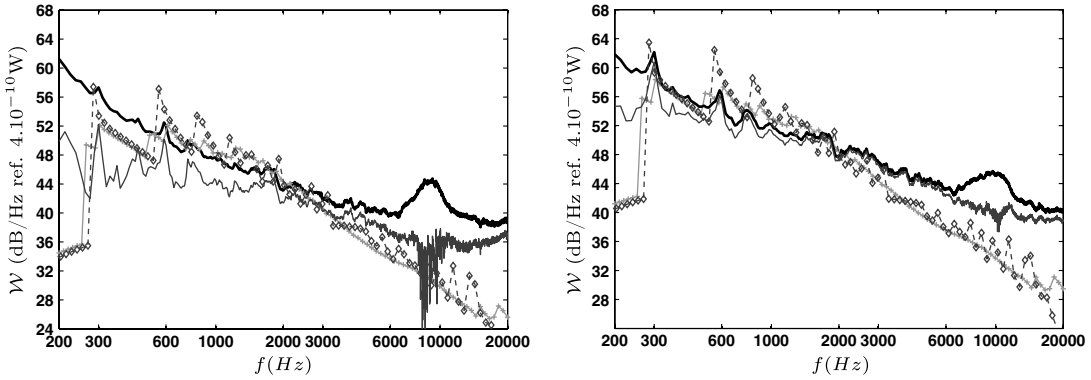

Fig. 12 PSD of the acoustic power [dB/Hz (reference 4×10^{-10} W)] at $U_{x_d} = 80$ m/s with cascade C2: from experimental data (thick black line), from corrected experimental data $\mathcal{L}_c$ (thin black line), from the quasi-three-dimensional formulation (dashed line with ◇) and from Hanson's approach (thin gray line with +): a) T1-C2 and b) T2-C2.

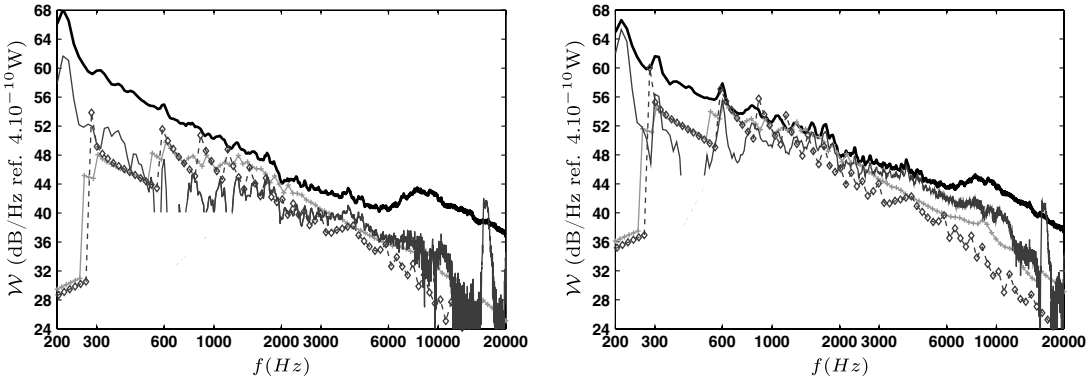

Fig. 13 PSD of the acoustic power [dB/Hz (reference 4×10^{-10} W)] at $U_{x_d} = 80$ m/s with cascade C1: from experimental data (thick black line), from corrected experimental data $\mathcal{L}_c$ (thin black line), from the quasi-three-dimensional formulation (dashed line with ◇) and from Hanson's approach (thin gray line with +): a) T1-C1 and b) T2-C1.

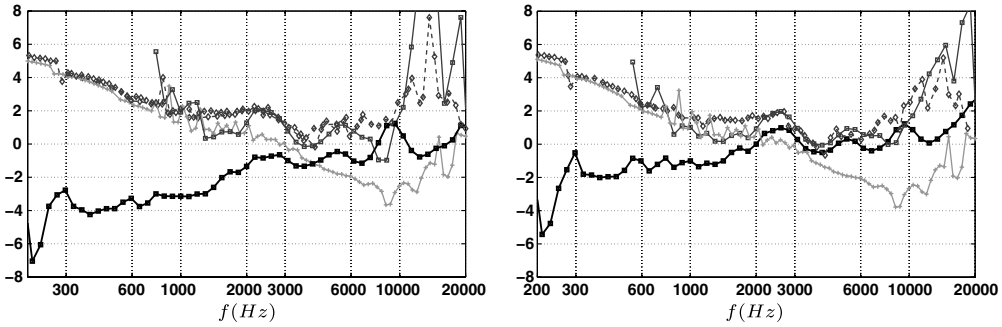

a) b)

Fig. 14 Difference of the PSD of the acoustic power between cascade C2 and cascade C1 from experimental data (thick black line with □), from corrected experimental data $\mathcal{L}_c$ (thin black line with □), from the quasi-3-D annular formulation (dashed line with ◇) and from Hanson's approach (thin gray line with +): a) with grid T1 and b) with grid T2.

density of modes leads to a smaller contribution of modes close to cutoff to the total noise.

The present quasi-3-D annular model follows the same trends as Hanson's model but exhibits sharper peaks. This rather good agreement suggests that the approximations introduced in Sec. V and the use of l_r give consistent results.

The predicted results do not agree so well with the uncorrected measurements for cascade C1, as shown in Fig. 13. With grid T2, the agreement between the measurements and Hanson's prediction is good for $f \in [0.6, 3]$ kHz, and the quasi-3-D annular formulation is about 1 to 2 dB lower. But for grid T1, both models underestimate the results by 2 and 3 dB, respectively, for $f \in [1, 5]$ kHz, by more than 4 dB elsewhere. Yet in this configuration, the models are in rather good agreement with the corrected measurements.

In the models, the effect of an increasing turbulence rate is a rather constant level increase over the whole spectrum, which is effectively mostly the case for cascade C2 in the experiment. Indeed, for cascade C2, the increase from 3% (grid T1) to 5.5% (grid T2) of turbulence intensity is about 4 to 5.5 dB in the frequency range $[0.6, 4]$ kHz whereas it is of 4 dB in $[4, 8]$ kHz in the experiment. The quasi-3-D annular model results are only lower by 0.2 dB. For cascade C1, the difference of 3.7 dB above 2.5 kHz found in the experiment is reproduced in the quasi-3-D annular model, but below this limit the behavior is less realistic, with a discrepancy of up to 3 dB. The discrepancy can be attributed to either an inaccuracy in the model, or the fact that the noise in the configuration C1-T1 is less easy to extract because of the contamination by self-noise or installation noise.

Above the measured drop of 3 dB at 2 kHz (for instance, Fig. 9), both models exhibit a steeper decay than the experiment with about −20 dB per decade instead of about −13 dB. The slower spectral decay in the experiment suggests that another mechanism might combine with the turbulence-interaction noise above 2 kHz.

To highlight the cascade effects and to make the interpretation of the figures easier, the comparisons with the experiment are performed now by plotting the difference between the PSDs of the cascades C2 and C1. This is done for the turbulence grid T1 in Fig. 14a and the turbulence grid T2 in Fig. 14b. For the sake of clarity, the peaks at cuton frequencies have been removed. Both models agree to predict that cascade C2 is noisier than cascade C1, whereas the uncorrected measurements lead to opposite trends. The discrepancy is larger with grid T1 and suggests a vertical offset over the whole frequency range. Conversely, the experimental results corrected according to the procedure of Sec. IV.B contradict the initial ones and are now in good agreement with the predictions. More precisely, both models reproduce the general decay of the difference with frequency below 4 kHz. But Hanson's model predicts an unrealistic monotonic decrease up to 9 kHz. In contrast, the present quasi-three-dimensional model correctly captures the humps above 2 kHz and the overall increase above 4 kHz. Therefore, the humps can be reasonably attributed to a three-dimensional effect of the annular geometry. However, additional sources of noise in the clean-inflow condition notably affect the relative effect of the configurations, therefore, all these conclusions are conditioned by the accuracy of the subtraction procedure.

VII. Conclusions

A preliminary experiment has been performed on a simple setup in order to assess an analytical model for the broadband noise produced by the impingement of turbulence on an annular cascade. The model resorts to a strip-theory to account for the three-dimensional geometry of the cascade. The unsteady loading on the blades is calculated at each radius from a previously published formulation for a three-dimensional rectilinear cascade, following Glegg's analytical approach. Finally, a Green's function tailored to the annular duct in uniform mean flow is used to describe the associated sound radiation.

The experimental setup has been designed for a more comprehensive study of the cascade effect on turbulence-ingestion noise. A single annular cascade is installed in an annular duct at the exit of an open-jet anechoic wind tunnel. Turbulence is generated by an adjustable grid mounted upstream of the nozzle.

Though simple, the setup involves additional sound sources associated with the flow developing over the duct surfaces. Therefore, a subtraction procedure has been applied to isolate the turbulence-interaction noise of the cascade. This reduced the frequency range of the investigations and led to focus on the variation of the sound when changing the parameters. Two vane numbers and two incident turbulence rates have been tested.

Simple hot-wire measurements have been performed to provide the statistical parameters of the turbulence used as input data in the model. Then the predictions of the acoustic power transmitted downstream in the duct have been compared with the radiated power deduced from far-field measurements, as well as to a simplified model proposed by Hanson.

Provided that a regularization procedure is applied to damp some numerical singularities inherent to the formulation, the proposed model is found to agree with the measured trends with a relative accuracy of less than 2 dB. Furthermore it reproduces three-dimensional effects that are not captured by the simplified model. This suggests that the underlying strip-theory approach coupled with a rectilinear-cascade response function and in-duct formulation is relevant for sound predictions in more complex 3-D turbomachinery configurations.

By the way the relatively small emergence of cascade noise in the experiment indicates that a very significant sound is generated as turbulence is convected past the annular edge of the exhaust duct. This mechanism probably occurs as well on real turbofan engine and should be considered when investigating broadband fan noise at exhaust.

It must be also noted that the present experiment addressed two cascades with different vane numbers but the same vane design, thus different loading conditions. A possible future work would be to investigate different cascades at equal aerodynamic performance.

Appendix A: Parameters of the Broadband Noise Model

The parameters and functions involved in Eq. (5) are defined as follows:

$$S^{\pm}_{m\mu}(r,\omega) = \left[-iq_3\frac{\mathrm{d}}{\mathrm{d}r} + \left(q_2\frac{m}{r} - q_1 k^{\pm}_{x,m\mu,R}\right)\right]E_{m,\mu}(r)$$

$$\zeta^{\pm}_{m,\mu}(r) = \frac{S^{\pm}_{m\mu}(r,\omega)}{E_{m,\mu}(r)} \tag{A1}$$

where $E_{m,\mu}(r)$ is the annular-duct eigen function defined in such a way that its square norm is $\Gamma_{m,\mu} = (R_T^2 - R_H^2)/2$. The associated eigen value is noticed $\chi_{m,\mu}$. $\mathbf{q}$ is the unit vector normal to the blade 0 at radius r in the duct reference frame. For zero sweep and lean, $q_3 = 0$. $E_{m,\mu}$ is expressed here in terms of Hankel functions for convenience:

$$E_{m,\mu} = C_{m,\mu}H_m^{(1)}(\chi_{m,\mu}r) + D_{m,\mu}H_m^{(2)}(\chi_{m,\mu}r) \tag{A2}$$

The wave number in the duct reference frame $\mathbf{K}_{d0}$ and the spanwise wave number $k_{z_{c0}}$ in the cascade reference frame $\mathcal{R}_c$ are

$$\mathbf{K}_{d,0} = (K_{x_{d0}}, \quad K_{y_{d0}}, \quad K_{z_{d0}}) = \left(\frac{\omega}{U_{x_R}}, \quad -\frac{m_g}{r}, \quad K_{z_{d0}}\right) \tag{A3a}$$

and

$$k_{z_{c0}} = Q_{31}K_{x_{d0}} + Q_{32}K_{y_{d0}} + Q_{33}K_{z_{d0}} \tag{A3b}$$

where $(Q_{i,j})(i,j) \in [1,3]2$ are the matrix elements of the matrix Q defined by Hanson [25].

The integrated contribution of the unsteady loading on the blades reads

$$Idp_{c,m,\mu}(\grave{r},\omega,k,k_{z_{c0}}) = \int_0^{c_d(r)} \Delta P_{c,0}\left(x_{cd}\cos\varphi(\grave{r})|\grave{r},k_{z_{c0}},-\frac{2\pi(m-kB)}{B},\omega\right) \times e^{i[k_{z_{c0}}\sin\varphi(\grave{r}) - k^{\pm}_{x,m\mu,cd}(\grave{r})]x_{cd}}\,\mathrm{d}x_{cd} \tag{A4}$$

where $\Delta P_{c,0}$ is the unsteady blade loading, made nondimensional by $\rho_0 c_0 u_{\mathrm{rms}}(\grave{r})$, produced by an incident vortical gust at the frequency ω, with spanwise wave number $k_{z_{c0}}$ and interblade phase angle $\sigma = -2\pi(m-kB)/B$, at the chordwise position $x_{cd}\cos\varphi(\grave{r})$ for the cascade geometry and mean flow at the duct radius $r = \grave{r}R_T$.

The wave numbers in the axial and chordwise directions in the reference frame $\mathcal{R}_{cd}$ before rotation of the sweep angle are

$$k^{\pm}_{x,m\mu,d} = \frac{-M_{x_d}k_0 \mp \kappa_{m,\mu}}{\beta^2_{x_d}} \qquad k^{\pm}_{x,m\mu,cd}(\grave{r}) = \cos\hat{\chi}k^{\pm}_{x,m\mu,d} - \sin\hat{\chi}\frac{m}{r} \tag{A5}$$

with $\kappa^2_{m,\mu} = k_0^2 - \beta^2_{x_d}\chi^2_{m,\mu}$. The wave numbers K_1 and K_2 are defined as

$$K_1 = -k^*_{z_{d1}} + k^{\pm}_{x,m\mu,d}\tan\hat{\varphi} - \frac{m}{r}\tan\hat{\psi}$$
$$K_2 = k_{z_{d1}} + k^{\pm}_{x,m\mu,d}\tan\hat{\varphi} - \frac{m}{r}\tan\hat{\psi} \tag{A6}$$

with

$$k_{z_{d1}} = -i\frac{\chi_{m,\mu}H_m^{(1)\prime}(\chi_{m,\mu}r)}{H_m^{(1)}(\chi_{m,\mu}r)} \tag{A7}$$

Appendix B: Coincidence of the Cutoff Frequencies

A correction of the quasi-3-D annular model can be proposed to remove the singularity at a duct-mode cutoff frequency. The spanwise wave number of the gust at this frequency is tuned to ensure the equality with the cascade-mode cuton frequency, $\omega_{c,m,\mu} = \omega_{\mathrm{ex},c,q}(k_{z_{c0}})$, leading to

$$\beta_{xd}\chi_{m,\mu}c_0 = \frac{c_0}{c\bar{s}^2}[M\bar{d}\sigma_q + \bar{s}_e\sqrt{\sigma_q^2 + \bar{k}^2_{z_{c0}}\bar{s}^2}]$$

where

$$m = m_g + qB, \qquad \sigma = -\frac{2\pi m_g}{B}, \qquad \sigma_q = \sigma - 2\pi q = -\frac{2\pi m}{B}$$

The overbar stands for rectilinear-cascade parameters made nondimensional with respect to the chord c. M is the chordwise Mach number, and s, d, s_e are lengths defined in Glegg's rectilinear-cascade model [20], reproduced below for completeness:

$$d = Q_{12}g, \qquad h = Q_{22}g, \qquad g = \frac{2\pi r}{B}, \qquad s = \sqrt{d^2 + h^2}$$
$$Mh = M_{xd}s, \qquad s_e = \beta_{xd}s \tag{B1}$$

In particular, s and d are the blade-to-blade distance at leading edges and the stagger distance in the cascade reference frame $\mathcal{R}_c$. After some manipulations, the spanwise wave number $k_{z_{c0}}$ is given by

$$k^2_{z_{c0}} = \left(\chi_{m,\mu} + \frac{mM_c}{\beta_{xd}r}\sin\chi\right)^2 - \frac{m^2}{r^2} \tag{B2}$$

The incident spanwise wave number can then be complex. In practice, this result is applied in a frequency band of 20 Hz around the cuton frequency of a duct mode.

Acknowledgments

The authors are grateful to Snecma for supporting the work and to P. Souchotte, P. Roland, and E. Jondeau from the Ecole Centrale de Lyon for their contribution to the measurements.

References

[1] Ganz, U. W., Joppa, P. D., Patten, T. J., and Scharpf, D. F., "Boeing 18-Inch Fan Rig Broadband Noise Test," NASA CR-1998-208704, 1998.

[2] Nallasamy, M., Envia, E., Thorp, S. A., and Shabbir, A., "Fan Noise Source Diagnostic Test—Computation of Rotor Wake Turbulence Noise," 8th AIAA/CEAS Aeroacoustics Conference and Exhibit, AIAA Paper 2002-2489, Breckenridge, CO, 2002; also NASA TM-2002-211798, Aug. 2002.

[3] Woodward, R. P., Hughes, C. E., Jeracki, R. J., and Miller, C. J., "Fan Noise Source Diagnostic Test—Far-Field Acoustic Results," 8th AIAA/CEAS Aeroacoustics Conference and Exhibit, AIAA Paper 2002-2427, Breckenridge, CO, 2002; also NASA TM-2002-211591, 2002.

[4] Envia, E., "Fan Noise Source Diagnostic Test—Vane Unsteady Pressure Results," 8th AIAA/CEAS Aeroacoustics Conference and Exhibit, AIAA Paper 2002-2430, Breckenridge, CO, 2002; also NASA TM-2002-211808, Aug. 2002.

[5] Heidelberg, L. J., "Fan Noise Source Diagnostic Test—Tone modal structure results," 8th AIAA/CEAS Aeroacoustics Conference and Exhibit, AIAA Paper 2002-2428 Breckenridge, CO, 2002; also NASA TM-2002-211594, May 2002.

[6] Hanson, D. B., "Mode Trapping in Coupled 2D Cascades-Acoustic and Aerodynamic Results," 15th Aeroacoustics Conference, AIAA Paper 93-4417, Long Beach, CA, Oct. 25–27 1993.

[7] Posson, H., and Roger, M., "Experimental Validation of a Cascade Response Function for Fan Broadband Noise Predictions," 14th AIAA/CEAS Aeroacoustics Conference and Exhibit, AIAA Paper 2008-2844, Vancouver, BC, Canada, 5–7 May 2008.

[8] Posson, H., Moreau, S., and Roger, M., "Fan-OGV Broadband Noise Prediction Using a Cascade Response," 15th AIAA/CEAS Aeroacoustics Conference and Exhibit, AIAA Paper 2009-3150, Miami, FL, 11–13 May 2009.

[9] Rienstra, S. W., "Acoustic Radiation from a Semi-Infinite Annular Duct in a Uniform Subsonic Mean Flow," *Journal of Sound and Vibration*, Vol. 94, No. 2, 1984, pp. 267–288. doi:10.1016/S0022-460X(84)80036-X

[10] Comte-Bellot, G., and Corrsin, S., "The Use of a Contraction to Improve the Isotropy of Grid-Generated Turbulence," *Journal of Fluid Mechanics*, Vol. 25, 1966, pp. 657–682.

doi:10.1017/S0022112066000338
[11] Hinze, J. O., *Turbulence*, McGraw–Hill, New York, 1959.
[12] Lordi, J., Homicz, G., and Rehm, R., "Effects of Finite Duct Length and Blade Chord on Noise Generation by a Rotating Blade Rows," AIAA 7th Fluid and Plasma Dynamics Conference, AIAA Paper 74-555, Palo Alto CA, June 17–19 1974.
[13] Arbey, H., "Contribution à L'Étude des Mécanismes de l'émission Sonore de Profils Aérodynamiques Placés dans des Écoulements Sains ou Perturbés," Ph.D. Thesis, Université Claude Bernard de Lyon, Lyon, France, 1981.
[14] Pope, S. B., *Turbulent Flows*, Cambridge University Press, Cambridge, England, U.K., 2000.
[15] Parker, R., "Resonance Effects in Wake Shedding from Parallel Plates: Calculation of Resonant Frequencies," *Journal of Sound and Vibration*, Vol. 5, No. 2, July 1967, pp. 330–343. doi:10.1016/0022-460X(67)90113-7
[16] Parker, R., "An Investigation of Acoustic Resonance Effects in an Axial Flow Compressor Stage," *Journal of Sound and Vibration*, Vol. 8, No. 2, Sept. 1968, pp. 281–297. doi:10.1016/0022-460X(68)90233-2
[17] Parker, R., and Price, D. C., "Wake Excited Resonances in an Annular Cascade: An Experimental Investigation," *Journal of Sound and Vibration*, Vol. 37, No. 2, May 1974, pp. 247–261. doi:10.1016/S0022-460X(74)80331-7
[18] Posson, H., and Roger, M., "Parametric Study of Gust Scattering and Sound Transmission Through a Blade Row," 13th AIAA/CEAS Aeroacoustics Conference and Exhibit, AIAA Paper 2007-3690, Rome, 21–23 May 2007.
[19] Posson, H., Roger, M., and Moreau, S., "Upon a Uniformly Valid Analytical Rectilinear Cascade Response Function," *Journal of Fluid Mechanics*, Vol. 663, Nov. 2010, pp. 22–52. doi:10.1017/S0022112010003368
[20] Glegg, S. A. L., "The Response of a Swept Blade Row to a Three-Dimensional Gust," *Journal of Sound and Vibration*, Vol. 227, No. 1, 1999, pp. 29–64. doi:10.1006/jsvi.1999.2327
[21] Peake, N., "The Interaction Between a High-Frequency Gust and a Blade Row," *Journal of Fluid Mechanics*, Vol. 241, 1992, pp. 261–289. doi:10.1017/S0022112092002039
[22] Posson, H., Moreau, S., and Roger, M., "On the Use of a Uniformly Valid Analytical Cascade Response Function for Broadband Noise Predictions," *Journal of Sound and Vibration*, Vol. 329, No. 18, Aug. 2010, pp. 3721–3743. doi:10.1016/j.jsv.2010.03.009
[23] Ventres, C. S., Theobald, M. A., and Mark, W. D., "Turbofan Noise Generation, Volume 1: Analysis," NASA CR-167952, 1982.
[24] Tyler, J. M., and Sofrin, T. G., "Axial Flow Field of an Axial Compressor Noise Studies," *Society of Automotive Engineers Transactions*, Vol. 70, 1962, pp. 309–332.
[25] Hanson, D. B., "Theory of Broadband Noise for Rotor and Stator Cascade with Inhomogeneous Inflow Turbulence Including Effects of Lean and Sweep," NASA CR-210762, 2001.
[26] Lansing, D. L., "Exact Solution for Radiation of Sound from a Semi-Infinite Circular Duct with Application to Fan and Compressor Noise," NASA SP-228, 1970.
[27] Namba, M., "Three-Dimensional Flows," *Manual of Aeroelasticity in Axial Flow Turbomachinery*, edited by M. F. Platzer, and F. O. Carta, Vol. 1, Unsteady Turbomachinery Aerodynamics, AGARD, Neuilly-sur-Seine, France, 1987, Chap. 4.
[28] Schulten, J. B. H. M., "Sound Generation by Ducted Fans and Propellers as a Lifting Surface Problem," Ph.D. Thesis, University of Twente, Enschede, The Netherlands, 1993.
[29] Atassi, H. M., Ali, A. A., Atassi, O. V., and Vinogradov, I. V., "Scattering of Incidence Disturbances by an Annular Cascade in a Swirling Flow," *Journal of Fluid Mechanics*, Vol. 499, 2004, pp. 111–138. doi:10.1017/S0022112003007031
[30] Hanson, D. B., and Horan, K. P., "Turbulence/Cascade Interaction: Spectra of Inflow, Cascade Response, and Noise," *4th AIAA/CEAS Aeroacoustics Conference and Exhibit*, AIAA, Reston, VA, 1998, pp. 688–700; also AIAA Paper 1998-2319, Toulouse, France, 1998.

E. Gutmark
Associate Editor